SIMULATION OF GAS FLOW BENEATH YUCCA MOUNTAIN, NEVADA, WITH A MODEL BASED ON THE FRESHWATER HEAD

Steven Amter
Benjamin Ross
Disposal Safety Incorporated
1660 L Street NW, Suite 314
Washington, DC 20036

ABSTRACT

Subsurface gas flow is relevant to the evaluation of the Yucca Mountain, Nevada site as a potential nuclear waste repository. The equations for this flow, formulated in terms of freshwater head, were solved by the finite-difference method using a spreadsheet program on a microcomputer. Cases solved were for current subsurface temperatures and a repository heated by 3, 14, and 30 K. Even a modest temperature increase of 14 to 30 K substantially increases the gas flux to the surface.

INTRODUCTION

Yucca Mountain, located at the border of the Nevada Test Site in a high desert region near Mercury, is being studied as a possible location for a high-level nuclear waste repository. The mountain is a steep-sided linear ridge and is underlain by a 500-m-thick unsaturated zone that is composed of alternating layers of ash flow and bedded tuffs (1). Intrinsic permeabilities in these formations are relatively high due to matrix fracturing.

Seasonal flows of air with velocities as high as 3.5 m/s have been observed (2) in deep boreholes at Yucca Mountain. These flows are attributed to convective circulation arising from topographic relief, seasonal temperature variation, and density differences resulting from variation in gas composition. Because air entering the mountain is drier than that within the mountain, evaporation and gas outflow result in vapor and fluid losses which, taken on the scale of the entire mountain, may be sizable.

Large-scale air flows may be significant to repository performance because they influence the distribution of carbon dioxide within the mountain and also result in a net flux of water vapor to the surrounding atmosphere. An understanding of the velocity, trajectories, and extent of mixing of the gas in Yucca Mountain is necessary both as input for a model of the carbon-14 distribution within the unsaturated zone (3) and for evaluation of the net vapor flux.

The density of a gas is dependent upon temperature, composition, and pressure. Temperatures inside Yucca Mountain vary much less than in the surrounding atmosphere, and the density of pore gas in the mountain reflects this. The composition of the gas in the mountain differs markedly from the atmosphere. Inside the mountain, the gas is generally saturated with water vapor, while the surrounding atmosphere is usually extremely dry. The gas inside the mountain also appears to contain more carbon dioxide than the atmosphere (4). Because water vapor is lighter than air, soil gas will be less dense than air at equal temperature. (The density effects of carbon dioxide are small compared to those of water vapor.)

In the winter, warmer, wetter gas inside the mountain results in a maximum density contrast with air in the atmosphere, and the highest flow velocities occur. The pattern of circulation is shown schematically in Fig. 1a. Dense air from the atmosphere displaces lighter air in the mountain, resulting in an outward flow of air at the top and an inward flow at the base. In the summer, gas inside the mountain is still wetter, but the temperature pattern is reversed. The density contrast is thus not as high as in the winter, and gas flow velocities are correspondingly lower. The general summertime pattern of flow is shown schematically in Fig. 1b. Cooler air inside the mountain sinks, resulting in inward flow at the top and outward flow at the base of the mountain. During the summer, when nighttime air temperatures may be lower than inside the mountain, low-velocity diurnal reversals of airflow sometimes occur in boreholes. The net flow, averaged over the year, resembles Fig. 1a but with a smaller magnitude than the winter flow.

Barometric pressure fluctuations also cause air to "breathe" in and out of the shallower portions of the mountain (5). This motion would not be expected to cause significant net movement of gas at depth; its effect on the mountain's water balance has yet to be evaluated.

In this paper, we calculate the steady-state gas flux through the interior of Yucca Mountain for a surface temperature, pressure, and humidity that roughly approximate the annual average. Gas fluxes are calculated for current subsurface temperatures and for several hypothetical cases in which the subsurface has been heated by a nuclear waste repository.

PREVIOUS WORK

Like water, air may flow in response to gradients of a number of fields, including temperature, density, pressure, gravitational potential, and chemical composition. However, gas is much more compressible than water, and density changes that result from variations in temperature and pressure are much more pronounced. This constrains our ability to apply simplifying assumptions (such as isothermal conditions) that "de-couple" the equations, and complicates the modeling of subsurface gas flow.

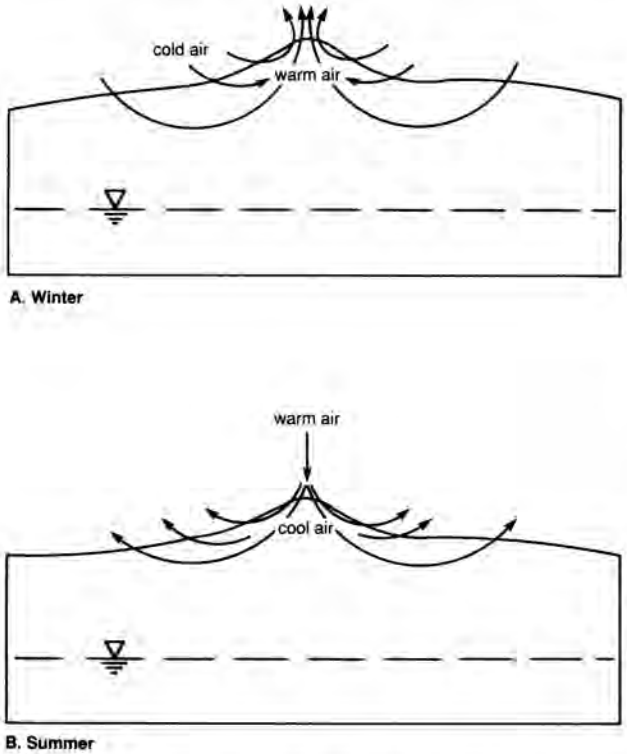

Fig. 1. Idealized Seasonal Gas Flow in the Subsurface at Yucca Mountain, Shown Schematically: (a) winter; (b) summer.

Numerical models of subsurface gas flow under the influence of temperature have been described by Pollock (6), Tsang and Pruess (7), and Kipp (8). The latter two models, like ours, were used to model cross-sections of Yucca Mountain.

The models of Pollock and Tsang and Pruess describe explicitly the coupling among temperature, mass flow of gas, mass flow of liquid water, and gas diffusion. At temperatures that approach or exceed the boiling point of water, all of these processes are important and must be included in a model.

At lower temperatures, and with reasonably small temperature gradients, gas diffusion becomes unimportant as a factor controlling gas flow. (See Appendix A.) At these temperatures, it is also reasonable to assume that liquid water fluxes are sufficient to maintain relative humidity near 100% everywhere. With these assumptions, the mass flow of gas can be related to the temperature alone and decoupled from liquid flow and diffusion.

In these circumstances, applying a model like those of Pollock and Tsang and Pruess would introduce unnecessary complexity. Furthermore, when the driving forces are topographic relief and variability in air temperature, pressure differences are smaller than in the circumstances analyzed by Tsang and Pruess. The two strongest forces acting on the soil gas, gravity and the pressure gradient resulting from the decrease of atmospheric pressure with increasing elevation, then very nearly cancel. If one were to model this situation by directly solving the system of governing equations, numerical problems associated with small numbers obtained by subtracting large numbers would be encountered.

The simpler approach in these circumstances is to model only the gas flow driven by temperature. Such a model was developed by Kipp (8), who adapted a variable-density flow simulator he had previously developed for water flow problems. The validity of the approximations in this model was not explicitly analyzed by Kipp and requires further examination.

In this paper, we present a model that also treats only temperature-driven flow but is based on a more rigorously derived governing equation. To avoid the numerical problems associated with the near-cancellation of the forces due to gravity and the pressure gradient, we expand the system of governing equations around reference values of temperature, pressure, and density. In doing so, we explicitly cancel the leading gravity and pressure-gradient terms. This process yields a single elliptic partial differential equation for a variable that resembles the "freshwater head" sometimes used by field hydrogeologists (9).

The application of our model to Yucca Mountain differs significantly from previous simulations of this system. Where previous models treated the tuff as uniform in permeability, we include an eastward-dipping bed of less permeable non-welded tuff. We also adopt, on the basis of measurements reported by Montazer et al. (5), a permeability for the welded tuff three orders of magnitude greater than that assumed by Tsang and Pruess (7). Unlike the previous workers who coupled models of heat and gas flow, we calculate gas flow from an assumed temperature distribution.

GOVERNING EQUATION

Deriving our governing equation requires the following assumptions about the physical system in the deep subsurface at Yucca Mountain.

- The gas behaves as an ideal gas.
- The gas is saturated with water vapor.
- Changes in partial pressure of water vapor are accommodated by changes in gas composition, with the total pressure remaining nearly constant (17).
- Gas viscosity is independent of pressure.
- Molecular diffusion resulting from gradients of water vapor partial pressure has a negligible effect on gas flow. This is demonstrated in Appendix A.
- All gas-filled voids in the matrix may be treated as a single porosity on time scales of years [see data of (5)].

- The unsaturated zone stays at constant saturation, with water lost to evaporation replenished by precipitation or from the water table.

The validity of these assumptions, with the possible exception of the final one, is well established. They imply that the system can be described by three equations, a volume balance equation, a constitutive relation, and Darcy's Law, as follows:

$$\nabla \cdot \mathbf{q} - \mathbf{q} \cdot \left[\left[\frac{1}{T}+\frac{1}{P_a}\frac{dP_v}{dT}\right]\nabla T - \frac{1}{P_a}\nabla P\right] = 0 \qquad \text{(Eq. 1)}$$

$$\rho = \frac{1}{RT}(P_v\Omega_v + P_a\Omega_a) \qquad \text{(Eq. 2)}$$

$$\mathbf{q} = -\frac{k}{\mu}(\nabla P - g\rho\hat{z}) \qquad \text{(Eq. 3)}$$

where q is the volumetric flux of gas (or Darcy velocity), T is the temperature, P is the pressure, P_v is the vapor pressure of water, P_a is defined by $P_a = P - P_v$, ρ is the gas density, R is the gas constant, Ω_a and Ω_v are the molar weights of dry air and water, respectively, k is the permeability of the rock, μ is the viscosity of the gas, g is the acceleration of gravity, and $\hat{z}$ is a downward-pointing unit vector.

To avoid the numerical problems associated with the subtraction of two large numbers to give a small number, we recast the problem in terms of a variable h defined by

$$h = \frac{P - P_o}{g\rho_o} - z$$

where P_o and ρ_o are reference values of pressure and density. A similar approach has been used in models of saline water flow, where h is known as the freshwater head (9-13). Darcy's Law then becomes

$$\mathbf{q} = -\frac{g\rho_o k}{\mu}(\nabla h - \rho'\hat{z}) \qquad \text{(Eq. 4)}$$

with h obtained by solving the governing equation

$$\nabla^2 h - m\nabla T \cdot \nabla h + \frac{1}{h_a}(\nabla h)^2 + \left[\frac{1}{T} + g\frac{\Omega_a - \Omega_v}{RT}\frac{dh_v}{dT} + \rho'\left(\frac{1}{T}+m\right)\right]\frac{\partial T}{\partial z} + \left[\frac{1-\rho'}{h_a} - \frac{g\Omega_a}{RT}\right]\frac{\partial h}{\partial z} - \frac{g\Omega_a}{RT} - \frac{\rho'}{h_a} + \frac{1}{k}\nabla k \cdot (\nabla h - \rho'\hat{z}) = 0 \qquad \text{(Eq. 5)}$$

where

$$\rho' = \frac{g}{RT}(h_v\Omega_v + h_a\Omega_a) - 1$$

$$m = \frac{1}{\mu}\frac{\partial \mu}{\partial T} + \frac{1}{T} + \frac{1}{h_a}\frac{dh_v}{dT}$$

$$h_v = P_v/g\rho_o$$

$$h_a = \frac{P_o}{g\rho_o} + z + h - h_v$$

We would like to simplify this equation by dropping small terms. Because this is an elliptical equation with small nonlinearities, we can compare the numerical values of first-order, zero-order, and constant terms and drop those that are small enough to be insignificant. Where these terms involve h or its derivatives, we use bounding values obtained from our subsequent solutions.

How small must a term be to be insignificant? Suppose that a temperature change of less than N would be insignificant. Any term can then be neglected if it changes (Eq. 5) less than does the temperature change of N - that is, if it is small compared to

$$\frac{g\Omega_a}{RT} - \frac{g\Omega_a}{R(T+N)} \cong \frac{g\Omega_a}{RT^2}N \qquad \text{(Eq. 6)}$$

To proceed any further requires numerical values. Physical constants are listed in Table I. Trial values of variables used in the elimination of small terms are listed in Table II. Variables, which are nearly constant within the range of expected values, have been evaluated at a reference point located inside Yucca Mountain, 375 m below the summit. This is midway to the water table at an elevation of approximately 1,075 m (1). All values are for current conditions (not heated by the waste).

With these values, (Eq. 6) can be evaluated as 3.8×10^{-9} N, with N in K. Because 1 K is small compared to both the

TABLE I

Physical Constants

constant	value
Ω_a	28.96 g mol^{-1}
Ω_v	18.02 g mol^{-1}
R	8.3144 x 10^7 g cm^2 s^{-2} mol^{-1} K^{-1}
g	980 cm s^{-2}

TABLE II

Reference Values for Comparison of Terms

Quantity	Value	Reference
T	300 K	16
∇T, $\frac{\partial T}{\partial z}$	2 x 10^{-4} K cm^{-1}	16
∇h, $\frac{\partial h}{\partial z}$	10^{-2}	this paper
$\frac{1}{\mu}\frac{\partial \mu}{\partial T}$	1.9 x 10^{-3} K^{-1}	18
h_a	8.5 x 10^5 cm	19
ρ'	0.040	this paper

geothermal temperature difference across the underground system and the uncertainty in predictions of average surface temperature, a temperature change of 1 K should be insignificant. Thus terms in (Eq. 5) whose value is 4 x 10^{-9} or smaller can be neglected.

We now return to (Eq. 5) and examine terms. The $(\nabla h)^2$ and (as some manipulation shows) $\partial h/\partial z$ terms are both between 10^{-10} and 10^{-9} and can be dropped. The ∇k term is zero except at boundaries between permeability zones, where it is given a special treatment discussed below; for the time being we will omit it. Other terms must be retained. In the smaller terms, however, the temperature T can be replaced by the reference temperature T_o. This yields the approximate governing equation

$$\nabla^2 h - m\nabla T \cdot \nabla h + \left[\frac{1}{T} + g\frac{\Omega_a - \Omega_v}{RT}\frac{dh_v}{dT} + \rho'\left[\frac{1}{T_o} + m\right]\right]\frac{\partial T}{\partial z} - \frac{g\Omega_a}{RT} - \frac{\rho'}{h^a} = 0 \quad \text{(Eq. 7)}$$

where

$$m = \frac{1}{\mu}\frac{\partial \mu}{\partial T}\bigg|_{T_o} + \frac{1}{T_o} + \frac{1}{h_a}\frac{dh_v}{dT}\bigg|_{T_o}.$$

In simulations with repository heating, the magnitudes of ∇T, ∇h, and ρ' can exceed the values shown in Table II. However, gas fluxes are much larger in these cases, and consequently the size which a term must attain to be significant also increases. We have used (Eq. 7) for all simulations reported in this paper.

PHYSICAL PROPERTIES OF THE SYSTEM

Gas flow was simulated in a two-dimensional vertical cross section across the area of the proposed nuclear waste repository. The location of the section is shown in Fig. 2, and its geometry is depicted in Fig. 3.

The mountain has a number of layers dipping approximately 6° to the east, with varying intrinsic permeabilities. The most important stratigraphic feature of the modeled section is the lower-permeability Paintbrush nonwelded tuff unit, which lies between thicker, more permeable welded tuff units.

Values of physical parameters used by the model are listed in Table III. The permeabilities are derived from (5); a permeability contrast between welded and nonwelded tuffs of a factor of 10 is assumed.

Four cases were simulated, each assuming different subsurface temperatures. In the "ambient" case, representing current conditions, the temperature T at any point in the subsurface was calculated from

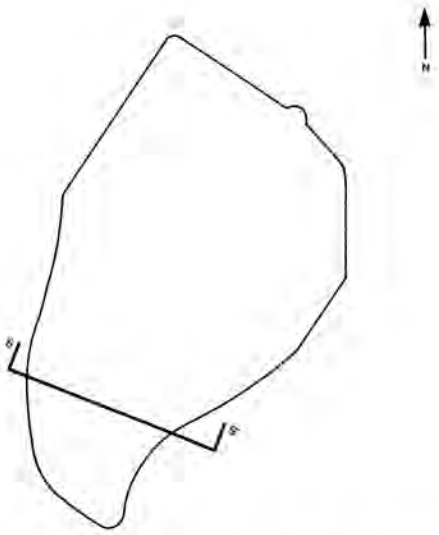

Fig. 2. Location of Cross Section Used in Simulation. Section Extends Along Line SS', and Continues to the West of S.

$$T = T_a + \gamma S_p \qquad \text{(Eq. 8)}$$

where

T_a is the air temperature

S_p is the difference in elevation between the point and the mountain peak

γ is the geothermal gradient.

With this approximation, the surface temperature along the flanks of the mountain slightly exceeded the annual-average atmospheric temperature. This may affect somewhat the near-surface lateral gas flows but will have less effect at depth.

In the remaining three cases, the subsurface was assumed to have been heated by the nuclear waste in the repository, raising temperatures 3, 14, and 30 K over ambient conditions. These are temperatures that might be expected thousands, tens of thousands, or perhaps hundreds of thousands of years in the future. (Compare Tsang and Pruess (7); note that Tsang and Pruess's use of a welded tuff permeability three orders of magnitude smaller than ours will cause convective heat transfer to be less and temperatures greater than if our value is correct.) For these simulations, temperatures at points above or below the repository were given by

$$T = T_a + \gamma S_p + \Delta T \frac{L}{S} \qquad \text{(Eq. 9)}$$

where ΔT is the temperature increase at the repository. The positive quantity L is the distance from the node to the repository, and S is the distance from the repository to the surface, both measured along a line perpendicular to the repository plane passing through the node. Temperatures at points to the side of the repository (strictly speaking, points from which a line drawn normal to the bedding would not intersect the repository) were always given by (Eq. 8).

The simulation region is surrounded by two boundary conditions:

- the mountain's atmospheric contact along its surface and

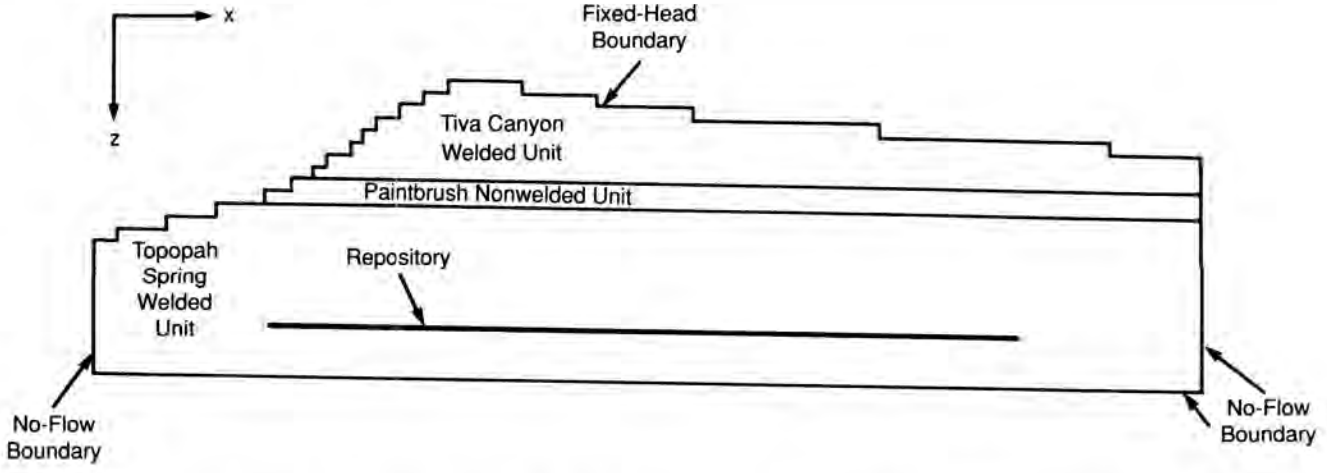

Fig. 3. Geometry of Cross Section Used in the Gas Flow Simulation. Adapted From S. Sinnock, Geologic Information System Product No. CAL0235, Sandia National Laboratories Unpublished Computer Output.

TABLE III

Values of Input Constants

Parameter	Symbol	Value	Reference
external temperature	T_a	294 K	--
reference fluid density	ρ_o	0.001007 g cm^{-3}	--
reference temperature	T_o	300 K	--
reference pressure	P_o	880,521 dyn cm^{-2}	--
viscosity at T_o	$\mu(T_o)$	1.86 x 10^{-4} g cm^{-1} s^{-1}	18
temperature coefficient of viscosity	$\frac{d\mu}{dT}$	3.5 x 10^{-7} g cm^{-1} s^{-1} K^{-1}	18
atmospheric relative humidity at z = 0	η	20%	
angle of dip	θ	6° or 0.10472 radians	1
geothermal gradient	γ	2 x 10^{-4} K cm^{-1}	5
intrinsic permeability of the Tiva Canyon and Topopah Spring Members	k_a , k_c	1.2 x 10^{-7} cm^2	5
intrinsic permeability of the non-welded and bedded tuff	k_b	1.2 x 10^{-8} cm^2	5

- no-flow conditions along the base, which lies a small distance above less permeable nonwelded and bedded tuff, and along portions of the sides.

The no-flow condition at the base of the simulated region has some physical basis because the permeability contrast would impede gas flow into the rocks below the Topopah Spring welded unit. The vertical no-flow boundaries were chosen for convenience.

The atmospheric boundary condition, representing a temperature and humidity that roughly approximate the annual average, is obtained by assuming that the mole fraction of water vapor in the *air is the same at* all elevations. (This assumption, rather than uniform relative humidity, is made to obtain a simpler formula.) Uniform temperature is also assumed. The boundary condition is then

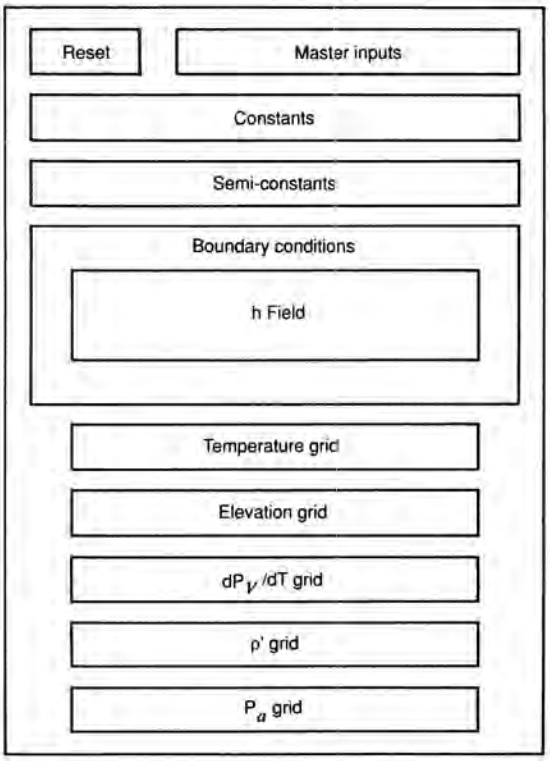

Fig. 4. Schematic Structure of the Head Solver Spreadsheet.

$$h = h_o \exp\left\{\left[\Omega_a + \eta\frac{h_v}{h_o}(\Omega_v - \Omega_a)\right]\frac{g\,z}{RT_a}\right\} \quad \text{(Eq. 10)}$$

$$- h_o - z$$

where

$h_o = P_o/g\rho_o$

η is the relative humidity outside the mountain at $z = 0$, and

P_o has been set equal to the atmospheric pressure at $z = 0$.

From the flux equation (4), the condition applied at no-flow boundaries is

$$\mathbf{q} \cdot \hat{\mathbf{n}} = -\frac{g\rho_o k}{\mu}\left[\frac{\partial h}{\partial n} - \rho'\hat{\mathbf{z}} \cdot \hat{\mathbf{n}}\right] = 0 \quad \text{(Eq. 11)}$$

where $\hat{\mathbf{n}}$ is a unit vector normal to the boundary.

NUMERICAL SOLUTION METHOD

The method of finite differences was used to obtain an approximate solution of (Eq. 7), using the boundary conditions and parameter values described in the previous section.

The flow field was discretized in a node-centered mesh scheme. A grid of approximately 2000 nodes, defining square blocks with 20-m sides, was constructed. The grid is parallel to the bedding plane (with a dip of 6° to the east) to simplify the implementation of internal layering and external boundary conditions.

The second-derivative term in (Eq. 7) was discretized using a standard 5-point formulation. Nodes lying on the contacts between units of differing permeability were treated by adding an additional term representing the effect of the ∇k term in (Eq. 5) when the gradient is zero except in an infinitesimally thin boundary layer. This treatment is an extension of the usual "refraction" of flow lines across boundaries.

The finite-difference equations were solved iteratively using the spreadsheet program SYMPHONY. Although not created for this purpose, spreadsheet programs make it possible to construct two-dimensional finite difference models from scratch with remarkable rapidity and ease (14, 15), without writing a line of code. Candidate models can be constructed, tested, modified, and if necessary discarded, saving the time and effort often wasted in writing computer codes for problems that have been wrongly formulated. Changes in the shape or size of the model can be accommodated with ease, while input and output are extremely efficient. Spreadsheet models, therefore, are useful in both relatively simple problems, where they can stand on their own, and also in complex problems, where they can aid in the development and verification of models that must later be rewritten in lengthy computer code.

The gas flux is calculated by two linked spreadsheets. Values of h are first calculated for the flow field on the "head solver sheet." These values are then sent to the "flux solver sheet," which calculates, separately, the two components of the flux vector.

Figure 4 is a schematic representation of a head solver sheet. At the heart of the model is the h field and associated boundary conditions. Here, the governing equation (Eq. 7) is solved for each node using Gauss-Seidel iteration. This is done by making each spreadsheet cell in the field correspond to a node of the model. The equation of each cell is the finite-difference equation for the corresponding node.

Note that the governing equation is not linear because it requires the value of ρ', which in turn also depends on the value of h. SYMPHONY uses the value of h from the last iteration in such a case. Because the governing equation

exceeds the maximum length of about 256 characters allowed by SYMPHONY, we created a separate ρ' grid. At nodes lying on boundaries between layers, the $\nabla h \cdot \nabla T$ term was omitted to make room for the additional "refraction" term.

Space-dependent constants in the governing equation, such as elevation and temperature, are obtained by referencing values from corresponding locations in the temperature and elevation grids. Constants, which do not vary in space, such as g, h_o, and T_o, are read from the field near the top of the sheet. To improve model efficiency by eliminating repetitive calculations, often-used combinations of constants and functions of constants are calculated in advance and stored in the area designated "semiconstants."

The model allows the user to change input values or boundary conditions at any time during model operation by setting values in the "master inputs" area at the top of the sheet, where parameters such as the angle of axis rotation, atmospheric temperature, and permeability of the various layers are stored. The model also allows the value of the h field to be uniformly set to any desired value before iteration, by using the reset option. This is accomplished by using an "IF/THEN/ELSE" type of logical operator in front of the governing equation.

The spreadsheet program displays current values of h on the computer screen while it is iterating. This display allows the analyst to examine the results for convergence and control the iteration process in real time.

Once the values of h have been calculated, fluxes are calculated by transferring values from the h, temperature, and elevation grids to the flux solver sheet. This spreadsheet uses a discretized version of (Eq. 7) to compute flux values. Because of the approximate treatment of layer boundaries, fluxes have not been calculated at these nodes.

Convergence of the four problems we solved required from 10 to 40 hr computation by an 80386-based microcomputer running at 16 MHz clock speed. The principal factor influencing variations in convergence time for this grid was the initial values of h; the longer convergence times were observed when h was initially set to zero at all nodes. (Readers selecting computer equipment should note that when the same problem was run on 80386/387 and 80286/287 computers, the computation speeds were directly proportional to the machines' clock speeds.)

RESULTS

Results of the four simulations are shown in Figs. 5 through 8. The figures depict gas flux vectors. Nodes where fluxes are too small to be displayed clearly are left blank. Note that the scale on Fig. 5 (current subsurface temperatures) differs from that on the other three figures; with identical scales, fluxes in Fig. 5 would be slightly smaller than those in Fig. 8.

As one would expect, gas fluxes increase with subsurface temperature. The range exceeds an order of magnitude.

The very large gas velocities observed at the repository margins in the higher-temperature cases are, in part, artifacts of the artificially sharp temperature change that was assumed at those locations. If a smoother and more realistic temperature transition were assumed, these velocities would be somewhat reduced, but there would still be a region of rapid flow in the same areas.

Kipp (8) developed a coupled model of gas flow and heat transfer under current conditions at Yucca Mountain. Our results shown in Fig. 5 can be compared with Kipp's results for similar temperature conditions; Kipp's gas fluxes are considerably larger. The discrepancy is largely accounted for by Kipp's use of permeabilities one order of magnitude larger than ours. The remaining discrepancy may be due to our use of an external temperature that exceeds Kipp's value by 1 K.

CONCLUSIONS

The calculations reported here agree qualitatively with the observation of Weeks (2) that there is a substantial upward gas flow at Yucca Mountain under ambient conditions. They also suggest that this flow would be accelerated considerably by even a modest amount of repository-induced heating.

If one assumes that the gas-filled porosity of the tuffs is 5% (16), the calculations indicate that the time needed for a particle of gas to travel from the repository elevation to the surface is on the order of 100 yr under current conditions. Repository heating could reduce this value considerably. These times cannot be used directly to characterize the movement of radioactive species such as carbon-14, because transport of these species will be slowed by chemical interactions with the aqueous and solid phases (3). More field work and modeling would be useful to better understand this system.

ACKNOWLEDGMENTS

We thank Scott Sinnock for providing stratigraphic cross-sections and Jeff Buchanan for generating computer graphic output. We also thank Roger S. Eaton, Todd C. Rasmussen, Martin S. Tierney, and Edwin P. Weeks for helpful discussions.

This work was supported by Sandia National Laboratories, as part of the Yucca Mountain Project, and Pacific Northwest Laboratories, as part of the Performance Assessment Scientific Support program. Both of these programs are supported by the U.S. Department of Energy.

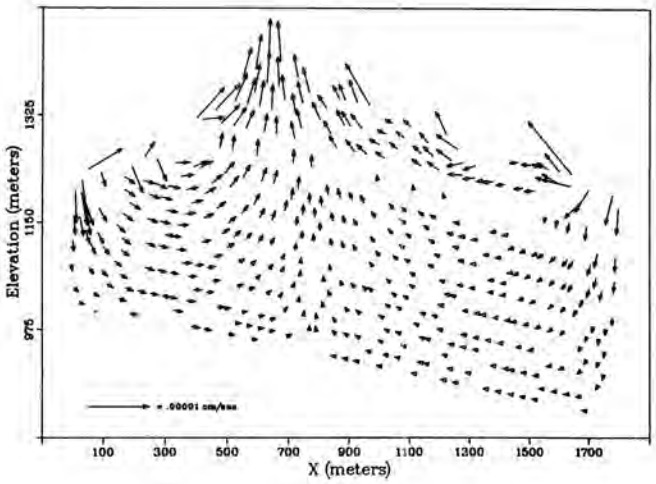

Fig. 5. Calculated Gas Fluxes With Current Subsurface Temperatures.

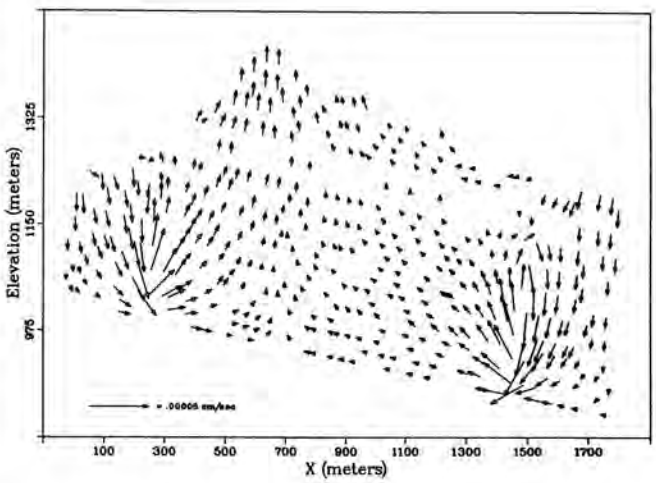

Fig. 7. Calculated Gas Fluxes With the Repository Heated by 14 K.

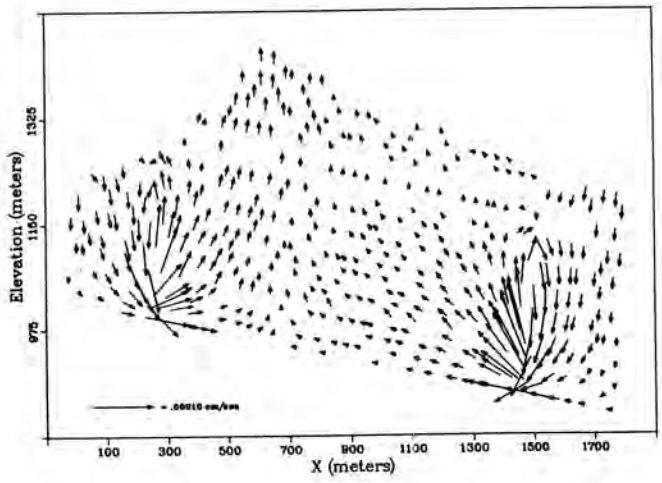

Fig. 6. Calculated Gas Fluxes With the Repository Heated by 30 K.

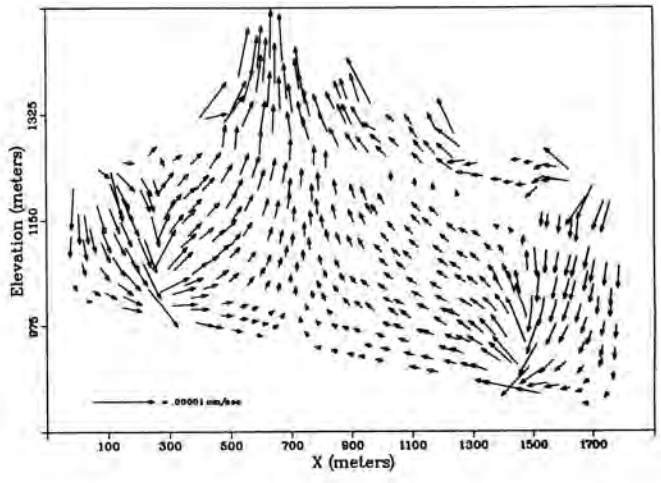

Fig. 8. Calculated Gas Fluxes With the Repository Heated by 3 K.

APPENDIX A

FLOW DRIVEN BY BINARY DIFFUSION

In the presence of a temperature gradient in the subsurface, there is a partial pressure gradient of water vapor because relative humidity in the deep subsurface is always close to 100%. Because the total pressure is approximately uniform (17), there will be a partial pressure gradient of the other components of air (referred to here as "dry air") in the opposite direction.

Evaporation and condensation will provide a source or sink of water vapor to maintain a steady-state diffusive flow. However, the countervailing diffusion of air requires a return flow to maintain a constant partial pressure. Consequently, a mass flow of air from higher to lower temperatures will be driven by this diffusion mechanism. This flow can be neglected because it is smaller than the temperature-driven flow.

To show this, one observes that the diffusion-driven mass flow of dry air, which is approximately equal to the total diffusion-driven flow, is equal in magnitude to the diffusion flux. The volumetric gas flux due to diffusion q is

$$q_d = \tau D n_D \gamma \frac{1}{P}\frac{dP_v}{dT}$$

where τ is the tortuosity, D is the diffusion constant, n_D is the drained porosity, γ is the temperature gradient, and $\frac{1}{P}\frac{dP_v}{dT}$ is the temperature derivative of the partial pressure of saturated water vapor as a fraction of ambient pressure.

Under ambient conditions, the temperature gradient is 2×10^{-4} K/cm. The derivative $\frac{1}{P}\frac{dP_v}{dT}$ is equal to about 2.2×10^{-3} K^1 at 30°C (18). Using a typical tortuosity of 0.1; a molecular diffusion constant for water vapor into air, corrected to ambient temperature and pressure, of 1000 m^2/yr (18); and a drained porosity of 0.05 a gas flux of about 4×10^{-10} cm/sec is obtained. This is negligible compared to the temperature-driven flow. Redoing the calculation at any of the higher temperatures considered in this analysis would not change this conclusion.

At yet higher temperatures, like those considered by Tsang and Pruess ((7), dP_v/dT becomes large enough to make diffusion-driven flow important. At such temperatures, the model presented here becomes inapplicable and a model that explicitly considers diffusion (such as that of Tsang and Pruess) must be used.

REFERENCES

1. R.B. SCOTT, and J. BONK, Preliminary geologic map of Yucca Mountain, Nye County, Nevada, with geologic sections, Open-File Report, U.S. Geological Survey, 84-494, Denver, CO, 1984.
2. E.P. WEEKS, Effect of topography on gas flow in unsaturated fractured rock - concepts and observations in Flow and Transport Through Unsaturated Fractured Rock, edited by D.D. Evans and T.J. Nicholson, Geophysical Monograph 42, American Geophysical Union, 1987, pp. 165-170.
3. B. ROSS, Gas-phase transport of carbon-14 released from nuclear waste into the unsaturated zone, in M.J. Apted and R.E. Westerman, eds., Scientific Basis for Nuclear Waste Management XI, Materials Research Society, Pittsburgh, 1988, pp. 273-284.
4. I.C. YANG, H.H. HAAS, E.P. WEEKS, and D.C. THORSTENSON, Analysis of gaseous-phase stable and radioactive isotopes in the unsaturated zone, Yucca Mountain, Nevada, in Proceedings of the NWWA Conference on Characterization and Monitoring of the Vadose (Unsaturated) Zone, Denver, November 19-21, 1985, pp. 488-506.
5. P. MONTAZER, E.P. WEEKS, F. THAMIR, S.M. YARD, and P.B. HOFRICHTER, Monitoring the vadose zone in fractured tuff, Yucca Mountain, Nevada, in Proceedings of the NWWA Conference on Characterization and Monitoring of the Vadose (Unsaturated) Zone, Denver, November 19-21, 1985, pp. 439-469.
6. D.W. POLLOCK, Simulation of fluid flow and energy transport processes associated with high-level radioactive waste disposal in unsaturated alluvium, Water Resour. Res., 32, 765-775 (1986).
7. Y.W. TSANG and K. PRUESS, A study of thermally induced convection near a high-level nuclear waste repository in partially saturated fractured tuff, Water Resour. Res., 23, 1958-1966 (1987).
8. K.L. KIPP, JR., Effect of topography on gas flow in unsaturated fractured rock - numerical simulation, in Flow and Transport Through Unsaturated Fractured Rock, edited by D.D. Evans and T.J. Nicholson, Geophysical Monograph 42, American Geophysical Union, 1987, pp. 171-176.
9. N.J. LUSCZYNSKI, Head and flow of water of variable density, J. Geophys. Res., 66, 4247-4256 (1961).
10. P. HUYAKORN and C. TAYLOR, Finite element models for coupled groundwater and convective dispersion. Proceedings of the 1st International Confer-

ence on Finite Elements in Water Resources, pp. 1.131-1.151, Pentech Press, London, 1976

11. E.O FRIND, Simulation of long-term transient density-dependent transport in groundwater, Adv. Water Resour., 5, 73-88, 1982.
12. P. HUYAKORN, J.W. MERCER, P.S. ANDERSEN, and H.O. WHITE, JR., Saltwater intrusion in aquifers: development and testing of a three-dimensional finite element model, Water Resour. Res., 23, 293-312, 1987.
13. P.B. DAVIES, Modeling a real, variable-density, ground-water flow - analysis of potentially significant errors, in Proceedings of the Solving Ground Water Problems with Models Conference and Exposition, Denver, February 10-12, 1987, pp. 888-903.
14. T.N. OLSTHOORN, The power of the electronic spreadsheet: modeling without special programs, Ground Water, 23, 381-390 (1985); Discussion, 24, 236-237, 1986.
15. W.R. HIGHLAND, Use of PC spreadsheet models as a routine analytical tool for solving ground water problems, in Proceedings of the Solving Ground Water Problems With Models Conference and Exposition, Denver, February 10-12, 1987, pp. 1345-1352.
16. P. MONTAZER, and W.E. WILSON, Hydrogeology of the unsaturated zone, Yucca Mountain, Nevada, in Proceedings of the NWWA Conference on Characterization and Monitoring of the Vadose (Unsaturated) Zone, Denver, CO, Nov. 19-21, 1985, pp. 396-412.
17. B. ROSS, A conceptual model of deep unsaturated zones with negligible recharge, Water Resour. Res., 20, 1627-1629, 1984.
18. R.C. WEAST, ed., CRC Handbook of Chemistry and Physics, 67th ed., CRC Press, Boca Raton, FL, 1986.
19. W.L. DONN, Meteorology, 4th edition, McGraw Hill, New York, 1975.